A Magnetohydrodynamic Boost for Relativistic Jets

Yosuke Mizuno[1,6], Philip Hardee[2], Dieter H. Hartmann[3], Ken-Ichi Nishikawa[1,4], and Bing Zhang[5]

ABSTRACT

We performed relativistic magnetohydrodynamic simulations of the hydrodynamic boosting mechanism for relativistic jets explored by Aloy & Rezzolla (2006) using the RAISHIN code. Simulation results show that the presence of a magnetic field may change the properties of the shock interface between the tenuous, overpressured jet (V_j^z) flowing tangentially to a dense external medium. Magnetic fields can lead to more efficient acceleration of the jet, in comparison to the pure-hydrodynamic case. A "poloidal" magnetic field (B^z), tangent to the interface and parallel to the jet flow, produces both a stronger outward moving shock and a stronger inward moving rarefaction wave. This leads to a large velocity component normal to the interface in addition to acceleration tangent to the interface, and the jet is thus accelerated to larger Lorentz factors than those obtained in the pure-hydrodynamic case. In contrast, a strong "toroidal" magnetic field (B^y), tangent to the interface but perpendicular to the jet flow, also leads to stronger acceleration tangent to the shock interface relative to the pure-hydrodynamic case, but to a lesser extent than found for the "poloidal" case due to the fact that the velocity component normal to the shock interface is now much smaller. Overall, the acceleration efficiency in the "toroidal" case is less than that of the "poloidal" case but both geometries still result in higher Lorentz factors than the pure-hydrodynamic case. Thus, the presence and relative orientation of a magnetic field in relativistic jets can significant modify the hydrodynamic boost mechanism studied by Aloy & Rezzolla (2006).

---

[1]National Space Science and Technology Center, 320 Sparkman Drive, VP 62, Huntsville, AL 35805, USA; Yosuke.Mizuno@msfc.nasa.gov

[2]Department of Physics and Astronomy, The University of Alabama, Tuscaloosa, AL 35487, USA

[3]302C Kinard Laboratory, Clemson University, Clemson, SC 29634-0978, USA

[4]Center for Space Plasma and Aeronomic Research, University of Alabama in Huntsville, Huntsville, AL 35899, USA

[5]Department of Physics, University of Nevada, Las Vegas, NV 89154, USA

[6]NASA Postdoctoral Program Fellow/ NASA Marshall Space Flight Center

Subject headings: black hole physics - galaxies: jets - gamma rays: bursts - magnetohydrodynamics: (MHD) - method: numerical -relativity

1. Introduction

Relativistic jets have been observed in active galactic nuclei (AGN) and quasars (e.g., Urry & Pavovani 1995; Ferrari 1998), in black hole binaries (microquasars) (e.g., Mirabel & Rodiriguez 1999), and are also thought to be responsible for the jetted emission from gamma-ray bursts (GRBs)(e.g., Zhang & Mészáros 2004; Piran 2005; Mészáros 2006). Proper motions observed in jets from microquasars and AGNs imply jet speeds from $\sim 0.9c$ up to $\sim 0.999c$, and Lorentz factors in excess of $\Gamma \sim 100$ have been inferred for GRBs. The acceleration mechanism(s) capable to boost jets to such highly-relativistic speeds have not yet been fully established.

Recently, Aloy & Rezzolla (2006) investigated a potentially very powerful acceleration mechanism in the context of purely hydrodynamical flows, posing a simple Riemann problem. If the jet is hotter and thus at higher pressure than the external medium, and moves with a large velocity tangent to the interface with a cold, slowly moving (or stationary) external medium, the relative motion of the two fluids produces a hydrodynamical structure in the direction perpendicular to the flow (normal to the interface), composed of a "forward shock" moving away from the jet axis, and a "reverse shock" (or a rarefaction wave) moving toward the jet axis. Following Aloy & Rezzolla (2006) we label this pattern either $_{\leftarrow}SCS_{\rightarrow}$, or $_{\leftarrow}RCS_{\rightarrow}$), where $_{\leftarrow}S$ refers to the reverse shock, ($_{\leftarrow}R$ to the reverse rarefaction wave), $S_{\rightarrow}$ to the forward shock, and C to the contact discontinuity between the two fluids. In the case $_{\leftarrow}RCS_{\rightarrow}$, the rarefaction wave propagates into the jet and the low pressure wave leads to strong acceleration of the jet fluid into the ultrarelativistic regime. This hydrodynamical boosting mechanism is very simple and powerful, but in addition to thermodynamic and kinematic effects one must also consider the effects of magnetic fields that may be present in the initial flow, or are generated within the shocked outflow.

The most promising mechanisms for producing relativistic jets involve magnetohydrodynamic centrifugal acceleration and/or magnetic pressure driven acceleration from the accretion disk around compact objects (e.g., Blandford & Payne 1982; Fukue 1990), or direct extraction of rotating energy from a rotating black hole (e.g., Penrose 1969; Blandford & Znajek 1977). Recent General Relativistic Magneto-Hydrodynamic (GRMHD) simulations of jet formation in the vicinity of strong gravitational field sources, such as black holes or neutron stars, show that jets can be produced and accelerated by the presence of magnetic fields which are significantly amplified by the rotation of the accretion disk and/or the

frame-dragging of a rotating black hole (e.g., Koide et al. 1999, 2000; Nishikawa et al. 2005; Mizuno et al. 2006b; De Villiers et al. 2005; Hawley & Krolik 2006; McKinney & Gammie 2004; McKinney 2006). The presence of strong magnetic fields is likely in areas close to the formation and acceleration region of relativistic jets. In the context of GRBs, standard scenarios invoke a fireball that is accelerated by thermal pressure during the initial free expansion phase (e.g., Mészáros et al. 1993; Piran et al. 1993). Magnetic dissipation may occur during the expansion, and a fraction of the dissipated energy may be used to further accelerate the fireball (e.g., Drenkhahn & Spruit 2002). Whether one considers the fate of the collapsing core of a very massive star (Woosley 1993), or the merger of a neutron star binary system (Paczynski 1986), the differentially rotating disks that feed the newly born black hole are likely to amplify any present seed field through magnetic breaking and the magnetorotational instability (MRI) proposed by Balbus & Hawley (1991, 1998). Numerical solutions of the coupled Einstein-Maxwell-MHD equations (e.g., Stephens et al. 2006, and references therein) confirm the expected growth of seed fields, even to the point at which the fields become strong enough to be dynamically important.

Here, we investigate the effect of magnetic fields on the boost mechanism proposed by Aloy & Rezzolla (2006). We show that the presence of magnetic fields in the jet can provide even more efficient acceleration of the jet than possible in the pure-hydrodynamic case. The highly significant role magnetic fields may play in accretion flows (e.g., Miller et al. 2006) and in core-collapse supernovae (e.g., Woosley & Janka 2005) is perhaps echoed in the collimated relativistic outflows from some compact stellar remnants.

2. Numerical Method

In order to study the magnetohydrodynamic boost mechanism for relativistic jets, we use a 1-dimensional special relativistic MHD (RMHD) version of the 3-dimensional GRMHD code "RAISHIN" in Cartesian coordinates (Mizuno et al. 2006a). A detailed description of the code and its verification can be found in Mizuno et al. (2006a). In the simulations presented here we use the piecewise parabolic method for reconstruction, the HLL approximate Riemann solver, a flux-CT scheme, and Noble's 2D method.

We consider the Riemann problem consisting of two uniform initial states (a left- and a right state) with different and discontinuous hydrodynamic properties specified by the rest-mass density ρ, the gas pressure p, the specific internal energy u, the specific enthalpy $h \equiv 1 + u/c^2 + p/\rho c^2$, and with velocity component $v^t = v^z$ (the jet-direction) tangent to the initial discontinuity. We consider the right state (the medium external to the jet) to be a cold fluid with a large rest-mass density and essentially at rest. Specifically, we select the following

initial conditions: $\rho_R = 10^{-2}\rho_0$, $p_R = 1.0\rho_0 c^2$, $v_R^n = v_R^x = 0.0$, and $v_R^t = v_R^z = 0.0$, where ρ_0 is an arbitrary normalization constant (our simulations are scale-fee) and c is the speed of light in vacuum, $c = 1$. The left state (jet region) is assumed to have larger pressure and lower density than the right state, and a relativistic velocity tangent to the discontinuity surface. Specifically, $\rho_L = 10^{-4}\rho_0$, $p_L = 10.0\rho_0 c^2$, $v_L^n = v_L^n = 0.0$, and $v_L^t = v_L^z = 0.99c$ ($\gamma_L \simeq 7$) (in Table 1 these conditions are collectively labeled as case HDA). Figure 1 shows a schematic depiction of the geometry of our simulations.

To investigate the effect of magnetic fields, we consider the following left state field geometries: "poloidal", $B^z = 3.0\sqrt{\rho_0 c^2}$ ($B_z^{'} = 3.0\sqrt{\rho_0 c^2}$), in the MHDA case, and "toroidal", $B^y = 21.0\sqrt{\rho_0 c^2}$ ($B_y^{'} = 3.0\sqrt{\rho_0 c^2}$), in the MHDB case (see Table1), where $B_i^{'}$ is the magnetic field measured in the jet fluid frame ($B_y^{'} = B^y/\gamma$, $B_z^{'} = B^z$). Although the strength of the magentic field measured in the laboratory frame (B^i) in the left state is larger in the MHDB case than the MHDA case, the magnetic pressure (p_{mag}) is the same as that of the MHDA case ($p_{mag} = (B^{'})^2/2$).

For comparison, the HDB case listed in Table 1 is a high gas pressure pure-hydrodynamic case ($p_L = 14.5\rho_0 c^2$). In this case the gas pressure p_L in left state is equal to the total pressure (p_{tot}) in the MHD cases ($p_{tot} = p_{gas} + p_{mag}$) in the left state. The fluid satisfies a $\Gamma - law$ equation of state with $\Gamma = 5/3$. We employ free boundary conditions in all-directions. The simulations are performed in the region $-0.2 \leq x \leq 0.2$ with 1200 computational zones until simulation time $t = 0.1$. We emphasize that our simulations are scale-fee. If we specify a system of size $L = 10^7$ cm ($\Delta L \simeq 8 \times 10^3$ cm), a simulation time of $t = 0.1$ corresponds to about 0.03 msec. The units of magnetic field strength and pressure depend on the normalization of the density. If we take, for example, the density unit to be $\rho_0 = 10^{-20}\,\mathrm{g\,cm^{-3}}$, the magnetic field strength unit is about 3 G and the pressure unit is $P \simeq 10\,\mathrm{dyn\,cm^{-2}}$.

3. Results

3.1. Effects of the magnetic field in 1-D simulations

Figure 2 shows the radial profiles of density, gas pressure, velocity normal to the interface (v^x) - hereafter normal velocity - and velocity tangent to the interface (v^z)- hereafter tangential velocity - for case HDA. The solution displays a right-moving shock, a right-moving contact discontinuity and a left-moving rarefaction wave ($_{\leftarrow}RCS_{\rightarrow}$). This hydrodynamical profile is similar to that found by Rezzolla et al. (2003) and Aloy & Rezzolla (2006). The simulation results (dashed lines) are in good agreement with the exact solution (solid lines,

calculated with the code of Giacomazzo & Rezzolla 2006) except for the spike in the normal velocity v^x. Otherwise the normal velocity and propagation of the shock propagating to the right (the forward shock) is $v^x \sim 0.065c$. The small spike evident in Fig. 2c is a numerical artifact and is seen in all simulation results (e.g., in the middle panel of Figs. 3) at the right moving shock ($S_{\rightarrow}$). In the left-moving rarefaction ($_{\leftarrow}R$) region, the tangential velocity increases as a result of the hydrodynamical boosting mechanism described by Aloy & Rezzolla (2006). In the case shown in Figure 2 the jet is accelerated to $\gamma \sim 17$ from an initial Lorentz factor of $\gamma_L \simeq 7$.

Figure 3 displays the resulting profiles of gas pressure, normal velocity (v^x) and tangential velocity (v^z) of the magnetohydrodynamic cases MHDA (blue), MHDB (red), and the high pressure, pure-hydrodynamic case HDB (green). In the magnetohydrodynamic cases, the magnetization parameter $\sigma \equiv b^2/\rho h$ and the plasma beta parameter $\beta \equiv p_{gas}/p_{mag}$ (on the left side) are 0.351 and 2.278, respectively. The resulting hydrodynamic structure consists of a right- propagating fast shock, a right-propagating contact discontinuity, and a left-propagating fast rarefaction wave ($_{\leftarrow}R_F C S_{F\rightarrow}$).

In the MHDA case ($B^z = 3.0$ ($B^{'}_z = 3.0$)) shown as blue curves, the right-moving fast shock ($S_{F\rightarrow}$) and the left-moving fast rarefaction wave ($_{\leftarrow}R_F$) are stronger than the related structures in the HDA case. Consequently, the normal velocity ($v^x \sim 0.096c$) is larger than that for the HDA case ($v^x \sim 0.059c$). The tangential velocity ($v^z \sim 0.9960c$) is lower than that of the HDA case ($v^z \sim 0.9965c$). Although the acceleration in the z-direction is weaker, the jet experiences a larger total acceleration than in the HDA case due to the larger normal velocity, and the jet Lorentz factor reaches $\gamma \sim 31$. Thus the "poloidal" magnetic field in the jet region strongly affects sideways expansion, shock profile and total acceleration.

In the MHDB case ($B^y = 21.0$ ($B^{'}_y = 3.0$)) shown as red curves, the right-moving fast shock ($S_{F\rightarrow}$) is slightly weaker than in the HDA case, and the resulting normal velocity ($v^x \sim 0.05590c$) is slightly less than in the HDA case ($v^x \sim 0.05890c$). The left-propagating fast rarefaction wave ($_{\leftarrow}R_F$) is slightly stronger than what we found for the HDA case. Therefore the tangential velocity ($v^z \sim 0.9973c$) is slightly higher than in the HDA case ($v^z \sim 0.9965c$). Thus the "toroidal" magnetic field in the jet region does not greatly affect the sideways expansion and shock profile, and the rsulting total acceleration to $\gamma \sim 20$ is only slightly larger than in the HDA case.

To investigate the effect of the total pressure, we performed a pure-hydrodynamic simulation with high gas pressure (case HDB), shown as green curves, equal to the total (gas plus magnetic) pressure ($p_{tot} = p_{gas} + p_{mag}$) in the MHD cases. The resulting structure for this case is the same as that of HDA case ($_{\leftarrow}RCS_{\rightarrow}$). The right-moving shock ($S_{\rightarrow}$) and the left-moving rarefaction wave ($_{\leftarrow}R$) are slightly stronger than those in the HDA case because

of the initial high gas pressure in left state. Consequently, the normal velocity v^x in the HDB case is larger ($v^x \sim 0.0645c$) than in the HDA case ($v^x \sim 0.0589c$). In the region of the left-propagating rarefaction wave ($_{\leftarrow}R$), the tangential velocity is increased only slightly, the jet acccelerates only with a marginally greater efficiency than in the HDA case, and the resultung Lorentz factor thus reaches only $\gamma \sim 19$.

Although the total pressure is the same in the HDB case and MHD cases, the existence and direction of the magnetic field changes the shock profiles and acceleration. We summarize the acceleration properties of the different cases in Table 2. When the gas pressure becomes large in the left state, the normal and tangential velocities increase and the jet is more efficiently accelerated. This is because the larger discontinuity in the gas pressure produces a stronger forward shock as well as stronger rarefaction. In MHD, the magnetic pressure is measured in the jet fluid frame and depends on the angle between the flow and magnetic field. The magnetosonic speeds also depend on the angle between the flow and the magnetic field, even for the same magnetic pressure. The direction of the magnetic field is thus a very important geometric parameter for relativistic magnetohydrodynamics. When a "poloidal" magnetic field (B^z) is present in the jet region, larger sideways expansion is produced, and the jet can achieve higher speeds due to the contribution from the normal velocity and changes in direction. By contrast, when a "toroidal" magnetic field (B^y) is present in the jet region, the shock profile is only changed slightly and the jet is only slightly more accelerated in the tangential direction due to the additional contribution of the tangential component of the Lorentz force ($\mathbf{F}_{EM,z} = (\mathbf{J} \times \mathbf{B})_z$) as shown in Fig. 4. It should be noted that there is no contribution by the thermal pressure gradient in the tangential direction. In Fig. 4, the region with high Lorentz force is different from the accelerated region as evidenced in the tangential velocity distribution of the MHDB case (red line of lower panel of Fig. 3). This is because the acceleration by the Lorentz force has happened at an earlier time in the simulation. From an efficiency point of view, a "poloidal" magnetic field provides the most efficient acceleration. A "toroidal" magnetic field with the same strength in the jet fluid frame and the same magnetic pressure as those of a "poloidal" field provides acceleration comparable to that resulting from high gas pressure, e.g., the HDB case.

3.2. Dependence of the MHD boost mechanism on the strength of magnetic field

To investigate the acceleration efficiency of the magnetic field, we compare jet speeds for the MHDA and MHDB cases, as shown in Fig. 5. The left panels of Fig. 5 shows the dependence of the maximum tangential and normal velocities and resulting Lorentz factors

on the strength of the poloidal ($B_z^{'}$) component of the magnetic field in the fluid frame. The solid line indicates values obtained using the code of Giacomazzo & Rezzolla (2006) and the crosses indicate values obtained from our simulations at the code time $t = 0.1$. Unfortunately an exact solution using the code of Giacomazzo & Rezzolla (2006) cannot be calculated for fields in excess of $B_z^{'} \simeq 14$ ($B^z = 14$) for numerical reasons. Also for numerical reasons our simulation does not yield a solution for $B_z^{'} > 4$ ($B^z > 4$) (the simulation results are indicated by +). When the poloidal magnetic field exceeds $B^z \sim 30$, the code of Giacomazzo & Rezzolla (2006) indicates that the maximum normal velocity increases and the maximum tangential velocity deceases, approximately linearly for both quantities. The break near $B_z^{'} \simeq 4$ occurs near the transition (in the left state) from gas pressure dominated to magnetic pressure dominated. It should be noted that in the hydrodynamic cases investigated by Aloy & Rezzolla (2006) the Lorentz factors decrease as the normal velocity increases (see their Fig. 4). However, our final Lorentz factor is different from that of Aloy & Rezzolla (2006), because their initial setting is different from our simulations. They vary the initial normal velocity in the jet region with constant jet Lorentz factor. The results shown in Figure 4 (left bottom panel) are caused by the presence of the poloidal magnetic field in the jet region and indicate that a sufficiently strong poloidal magnetic field in the jet region will allow a jet to achieve $\gamma \sim 300$, even if the jet is only "mildly" relativistic initially, i.e., $\gamma_L \sim 7$.

The right panels of Fig. 5 show the dependencies of the maximum tangential and normal velocities and the Lorentz factor on the strength of the toroidal ($B_y^{'}$) component of the magnetic field in the fluid frame. Again, the solid line indicates values obtained with the code of Giacomazzo & Rezzolla (2006) and the crosses indicate values obtained from our simulation at the simulation time $t = 0.1$. When the toroidal magnetic field becomes large in the jet region, the maximum normal velocity deceases and the maximum tangential velocity increases. This dependence is opposite to that of the poloidal magnetic field. The acceleration in the tangential direction occurs due to the additional contribution of the Lorentz force as shown in Fig. 4. When the toroidal magnetic field becomes large in the jet region, the Lorentz force in the tangential direction increases and contributes to the large acceleration of the jet in the tangential direction. The transition from gas pressure dominated to magnetic pressure dominated left states occurs near $B_y^{'} \simeq 4$. The change of properties around $B_y^{'} \simeq 4$ is clearly seen in the profile of maximum tangential velocity. The acceleration is much less than that found in the comparable poloidal magnetic field case. While at $B_z^{'} \simeq 14$ the maximum Lorentz factor reaches $\gamma \sim 300$, at $B_y^{'} \simeq 14$ the maximum Lorentz factor is only $\gamma \sim 66$. Thus, a poloidal magnetic field provides ab about 5 times larger increase in the maximum Lorentz factor in comparison to a toroidal magnetic field.

We extended the computation of maximum tangential and normal velocities and the maximum Lorentz factor in the toroidal case, indicating a continuing linear increase of the

maximum Lorentz factor to ($\gamma \sim 600$) as the field approaches $B_y^{'}(\sim 128)$ (not shown here). The Lorentz factor is ~ 300 at $B_y^{'} \sim 57$, which is about 4 times larger than $B_z^{'} \simeq 14$.

3.3. Multidimensional simulations

To investigate the effects induced by more than one degree of freedom, we perform two dimensional RMHD simulations of the MHDA case ($B_z^{'} = 3.0$). The computational domain corresponds to a local part of the jet flow. In the simulations, a "pre-existing" jet flow is established across the computational domain. The inital condition is the same as that of the 1D MHDA case (e.g., $v^z = 0.99c$ and $B_z^{'} = 3.0$). In order to investigate a possible influence of the chosen coordinate system, we perform the calculations in Cartesian and cylindrical coordinates. The discontinuities between the jet and the external medium are set at x or $r = 1.0$ in the inital state (see Fig. 1).

The computational domain is $0 \leq x, r \leq 2.0$ and $0 \leq z \leq 5.0$ with $(N_{x,r} \times N_z) = (800 \times 250)$, where $N_{x,r}$ and N_z are the computational zone number in the x or r direction and in the z direction. In order to handle the shock profile with high spatial resolution, we use large numbers of computational zones in the x or r direction. We impose periodic boundary conditions on the z-direction and outflow boundary conditions on the x or r direction.

Figure 6 shows 2D images of the Lorentz factor for the 2D MHDA in Cartesian and in cylindirical coordinates at time $t = 1.0$. In both of cases, the edge of the jet region is accelerated by the MHD boost mechanism and reaches a maximum Lorentz factor of more than 30 from an initial Lorentz factor $\gamma_L \simeq 7$. The jets in cylindrical coordinates are slightly more efficiently accelerated than the jets in Cartesian coordinates.

In order to investigate simulation results quantitatively, we take one-dimensional cuts through the computational box parallel to the z-axis. Figure 7 shows the resulting profiles of gas pressure, Lorentz factor (γ), normal velocity (v^x or v^r) and tangential velocity (v^z) of 2D MHDA in Cartesian and in cylindrical coordinates cases. The result consists of a right-moving fast shock, right-moving contact discontinuity, and a left-moving fast rarefaction wave ($_{\leftarrow}R_F C S_{F\rightarrow}$). The profiles from the 2D MHDA simulation in Cartesian coordinates match well those of the 1D MHDA case. In the 2D MHDA simulation with cylindrical coordinates, the right-moving fast shock ($S_{F\rightarrow}$) is weaker and the left-moving fast rarefaction wave ($_{\leftarrow}R_F$) is stronger than those of the 2D MHDA simulations with Cartesian coordinates. Selecting cylindrical coordinates, causes the normal velocity to decrease gradually in the expansion. The tangential velocity ($v^z \sim 0.99595c$) is slightly faster than that of 2D MHDA in Cartesian coordinates ($v^z \sim 0.99610c$). Because the acceleration in the z-direction is stronger, the jet

is more accelerated than in 2D MHDA simulations using Cartesian coordinates, and the jet Lorentz factor reaches $\gamma \sim 38$. Therefore, we find that different coordinate systems affect the sideways expansion, shock profile, and acceleration. The current simple 2D MHD simulation in cylindrical coordinates is directly applicable to a 3D cylindrical geometry where the magentic field and jet flow are aligned and tangent to the jet-external medium interface. However, recent GRMHD simulations of jet formation predict that the jet has a rotational velocity (e.g., Nishikawa et al. 2005; Mizuno et al. 2006b; De Villiers et al. 2005; Hawley & Krolik 2006; McKinney & Gammie 2004; McKinney 2006). In order to investigate the full-3D effects, we will perform 3D RMHD simulations with helical field in the future.

4. Summary and Discussion

We performed relativistic magnetohydrodynamic simulations of an acceleration boosting mechanism for fast astrophysical jet flows that result from highly overpressured, tenuous flows with an initially modest relativistic speed relative to a cold, dense external dense medium at rest. We employed the newly developed RAISHIN code (Mizuno et al. 2006a), to study the relativistic boost mechanism proposed by Aloy & Rezzolla (2006), who showed that hydrodynamic accelerations to $\gamma > 1000$ are possible in the situation described above. For numerical reasons, we reduced the initial discontinuity in the pressure and also reduced the initial jet velocity. Our results still show the same behavior ($_{\leftarrow}RCS_{\rightarrow}$) found in Rezzolla et al. (2003) and Aloy & Rezzolla (2006). The same hydrodynamical structures emerge in our simulation, confirming the basic properties of the boost mechanism proposed in their work. We extend their study with relativistic MHD simulations to investigate the effects of magnetic fields which are ubiquitous in relativistic jets.

Our simulations show that the presence of a magnetic field in the jet can significantly change the properties of the outward moving shock and inward moving rarefaction wave, and can in fact result in even more efficient acceleration of the jet than in a pure-hydrodynamic case. In particular, the presence of a poloidal magnetic field along the jet and parallel to jet flow produces a stronger outward moving shock and inward moving rarefaction wave. This leads to acceleration from $\gamma \sim 7$ to $\gamma \gtrsim 30$ when the magnetic pressure is comparable to the gas pressure. A comparable pure-hydrodynamic case yields acceleration to $\gamma \lesssim 20$. Our results would indicate acceleration to $\gamma \sim 300$ for magnetic pressure ten times the gas pressure. Thus, the magnetic field can in principle play an important role in this relativistic jet boost mechanism. To address the question whether or not such strong, magnetically enhanced boosts really do take place in astrophysical sources (AGNs, quasars, microquasars, gamma-ray bursts) will require additional studies that link the radiation processes in such

high-Γ flows to observables. The operation of the MHD boost is likely to be strongly affected by the properties of the external medium, and it is conceivable that magnetic effects kick in strongly in GRB sources but are absent in the environs of super-massive black holes of the cores of galaxies.

We found that jets modeled with polar coordinates are more acclerated than those in Cartesian coordinates. Our 1D and 2D results for a poloidal field component are likely to be directly applicable to a comparable 3D cylindrical geometry where the magnetic field and jet flow are aligned and tangent to the jet-external medium interface. However, our present results for the 1D toroidal field component are not likely to apply in a 3D cylindrical geometry where a toroidal field component exhibits hoop stress that does not exist in the 1D configuration. It seems likely that this hoop stress would so modify the sideways expansion of an overpressured cylindrical jet as to render our present toroidal field results not applicable unless the magnetic field in 3D is tangled. In this case the magnetic pressure would behave similarly to the toroidal 1D case computed here. In order to investigate the full 3D effects, we will perform full 3D RMHD simulations with helical field in future studies.

A hot GRB fireball can expand and accelerate under its thermal pressure to reach large Lorentz factors as long as baryon-loading is small (Mészáros et al. 1993; Piran et al. 1993). Although this simple model can account for the large (> 100) Lorentz factors inferred for GRBs, it does not reflect more realistic settings of complex GRB progenitor/central engine models. In the collapsar model for long-duration GRBs (Woosley 1993), the tenuous jet is believed to propagate in a surrounding dense stellar envelope (Zhang et al. 2003), so that the hydrodynamic configuration considered by Aloy & Rezzolla (2006) and in this paper is naturally satisfied. A strong poloidal magnetic field is likely present at the bottom of the central engine. The magnetohydrodynamic boost mechanism discussed here would then play an important role in jet acceleration. The final Lorentz factor should depend on the detailed parameters invoked in this mechanism as well as the unknown baryon loading process during the propagation of the jet in the envelope. In the case of short GRBs that may be of compact star merger origin (e.g., Paczýnski 1986), there is no dense stellar envelope surrounding the jet. The jet region is nonetheless more tenuous than the surrounding medium due to the centrifugal barrier in the jet, so that the acceleration mechanism discussed here still applies (e.g., see Aloy et al. 2005 for the pure hydrodynamic case). Due to a likely smaller baryon loading in the merger environment, the jet may achieve an even higher Lorentz factor than for the case of long GRBs, as suggested by some observations (e.g. their harder spectrum and shorter spectral lags). The magnetohydrodynamic acceleration mechanism discussed here also naturally yields a GRB jet with substantial angular structure. In particular, since acceleration is favored in the rarefaction region near the contact discontinuity, this mechanism naturally gives rise to the kind of ring-shaped jet that has been discussed in some

empirical GRB models (e.g. Eichler & Levinson 2006).

Y. M. is supported by an appointment of the NASA Postdoctoral Program at NASA Marshall Space Flight Center, administered by Oak Ridge Associated Universities through a contract with NASA. P. H. acknowledges partial support by National Space Science and Technology Center (NSSTC/NASA) cooperative agreement NCC8-256 and NSF award AST-0506666 to the University of Alabama. K. N. acknowledges partial support by NSF awards ATM-0100997, INT-9981508, and AST-0506719, and the NASA award NNG05GK73G to the University of Alabama in Huntsville. B. Z. acknowledges partial support by NASA award NNG05GB67G and NNG06GH62G. The simulations have been performed on the IBM p690 at the National Center for Supercomputing Applications (NCSA) which is supported by the NSF and Altix3700 BX2 at YITP in Kyoto University.

REFERENCES

Aloy, M. A., Janka, H.-T. & Müller, E. 2005, A&A, 436, 273

Aloy, M. A. & Rezzolla, L. 2006, ApJ, 640, L115

Balbus, S. A., and Hawley, J. F. 1991, ApJ 376, 214

Balbus, S. A., and Hawley, J. F. 1998, Rev. Mod. Phys. 70, 1

Blandford, R. D. & Znajek, R. L. 1977, MNRAS, 179, 433

Blandford, R. D. & Payne, D. G. 1982, MNRAS, 199, 883

De Villiers, J.-P., Hawley, J. F., Krolik, J. H., & Hirose, S. 2005, ApJ, 620, 878

Drenkhahn, G., & Spruit, H. C. A&A, 391, 1141

Eichler, D. & Levinson, A. 2006, ApJ, 649, L5

Giacomazzo, B. & Rezzolla, L. 2006, J. Fluid Mech., 562, 223

Hawley & Krolik 2006, ApJ, 614, 103

Koide, S., Shibata, K., Kudoh, T. 1999, ApJ, 522, 727

Koide, S., Meier, D. L., Shibata, K., & Kudoh, T. 2000, ApJ, 536, 668

McKinney, J. C. 2006, MNRAS, 368, 1561

McKinney, J. C. & Gammie, C. F. 2004, ApJ, 611, 977

Mészáros, P. 2006, Rep. Prog. Phys., 69, 2259 (astro-ph/0605208)

Mészáros, P., Laguna, P. & Rees, M. J. 1993, ApJ, 415, 181

Miller, J. M., et al. 2006, Nature 441, 953

Mizuno, Y., Nishikawa, K.-I., Koide, S., Hardee, P., & Fishman, G. J. 2006a, ApJS, submitted (astro-ph/0609004)

——. 2006b, ApJ, submitted (astro-ph/0609344)

Nishikawa, K.-I., Richardson, G., Koide, S., Shibata, K., Kudoh, T., Hardee, P., & Fishman, G. J. 2005, ApJ, 625, 60

Paczýnski, B. 1986, ApJ, 308, L43

Penrose, R. 1969, Nuovo Cimento, 1, 252

Piran, T. 2005, Reviews of Modern Physics, 76, 1143

Piran, T., Shemi, A. & Narayan, R. 1993, MNRAS, 263, 861

Rezzolla, L., Zanotti, O., & Pons, J. A. 2003, J. Fluid Mech., 479, 199

Stephens, B. C., Duez, M. D., Liu, Y. T., et al., Class. Quantum Grav., submitted (arXiv:gr-qc/0610103)

Woosley, S. E. 1993, ApJ, 405, 273

Woosley, S. E., and Janka, H.-T. 2006, Nature Physics, 1, 147

Zhang, B. & Mészáros, P. 2004, Int. J. Mod. Phys., A19, 2385 (astro-ph/0311321)

Zhang, W., Woosley, S. E. & MacFadyen, A. I. 2003, ApJ, 586, 356

Table 1. Model and Parameters

Case		ρ	p	v^x	v^y	v^z	$B^x(B^{'}_x)$	$B^y(B^{'}_y)$	$B^z(B^{'}_z)$
HDA	*left state*	10^{-4}	10.0	0.0	0.0	0.99	0.0(0.0)	0.0(0.0)	0.0(0.0)
	right state	10^{-2}	1.0	0.0	0.0	0.0	0.0(0.0)	0.0(0.0)	0.0(0.0)
HDB	*left state*	10^{-4}	14.5	0.0	0.0	0.99	0.0(0.0)	0.0(0.0)	0.0(0.0)
	right state	10^{-2}	1.0	0.0	0.0	0.0	0.0(0.0)	0.0(0.0)	0.0(0.0)
MHDA	*left state*	10^{-4}	10.0	0.0	0.0	0.99	0.0(0.0)	0.0(0.0)	3.0(3.0)
	right state	10^{-2}	1.0	0.0	0.0	0.0	0.0(0.0)	0.0(0.0)	0.0(0.0)
MHDB	*left state*	10^{-4}	10.0	0.0	0.0	0.99	0.0(0.0)	21.0(3.0)	0.0(0.0)
	right state	10^{-2}	1.0	0.0	0.0	0.0	0.0(0.0)	0.0(0.0)	0.0(0.0)

Note. — Initial conditions for the simulations. HDA is hydrodynamic case. MHDA and MHDB are magnetohydodynamic cases with $B^z_L = 3.0$ ($B^{'}_{z,L} = 3.0$) and $B^y_L = 21.0$ ($B^{'}_{y,L} = 3.0$) respectively. HDB is hydrodynamic case with gas pressure $p_{gas,L}$ equal to total pressure ($p_{tot,L} = p_{gas,L} + p_{mag,L}$) of MHD cases.

Table 2. Maximum velocities and Lorentz factor

Case	v^x	v^z	γ
HDA	0.0588980	0.996500	16.8570
HDB (high gas pressure)	0.0645304	0.996593	19.4660
MHDA (poloidal field)	0.0956877	0.995931	31.4377
MHDB (toroidal field)	0.0559023	0.997260	20.6427

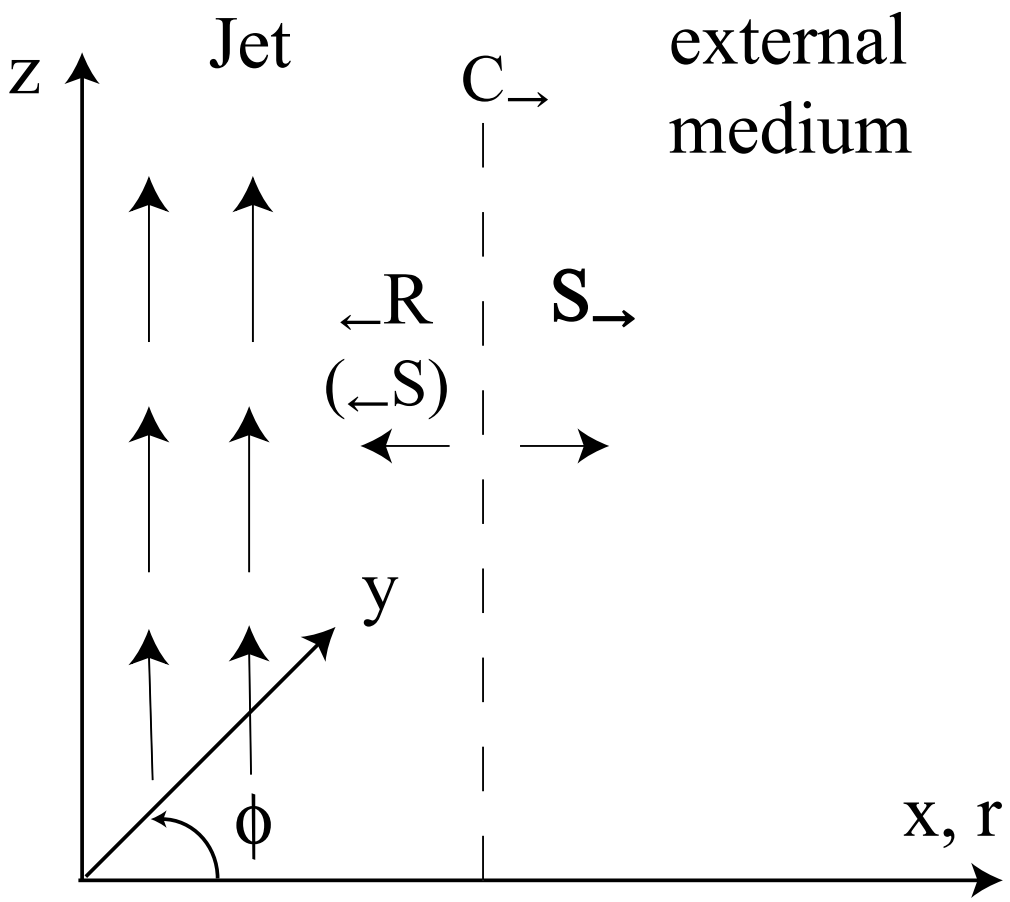

Fig. 1.— Schematic picture of our simulations.

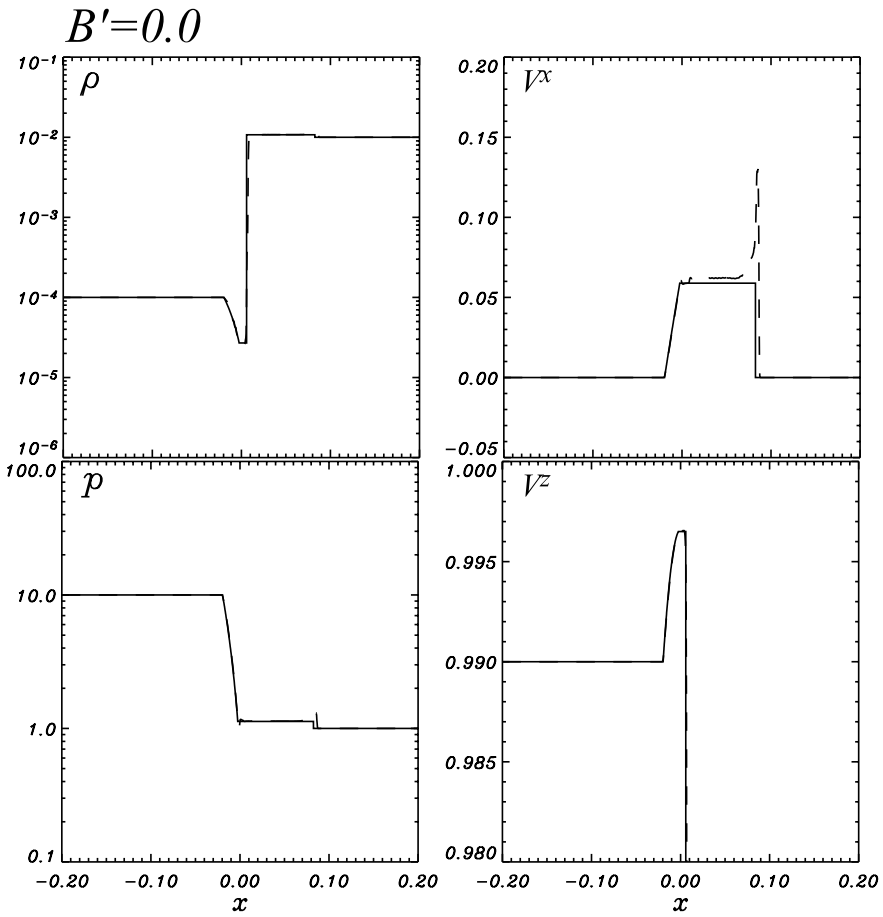

Fig. 2.— Profiles of (*left-upper panel*) density, (*left-lower panel*) gas pressure, (*right-upper panel*) normal velocity (v^x), and (*right-lower panel*) tangential velocity (v^z) of HDA case at time $t = 0.1$. The solid lines are the exact solution and the dashed lines are the simulation results.

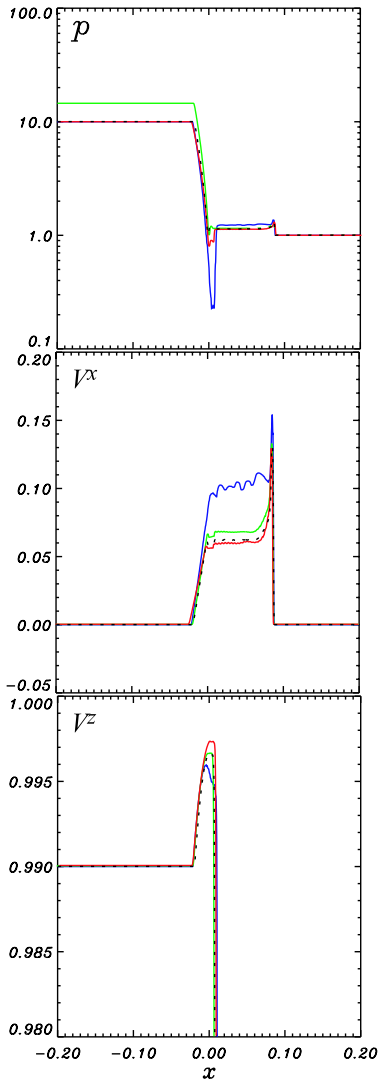

Fig. 3.— Profiles of gas pressure (*upper panel*), normal velocity (v^x) (*middle panel*), and tangential velocity (v^z) (*lower panel*) of HDB (green), MHDA (blue), MHDB (red), and HDA (dotted-line) at time $t = 0.1$.

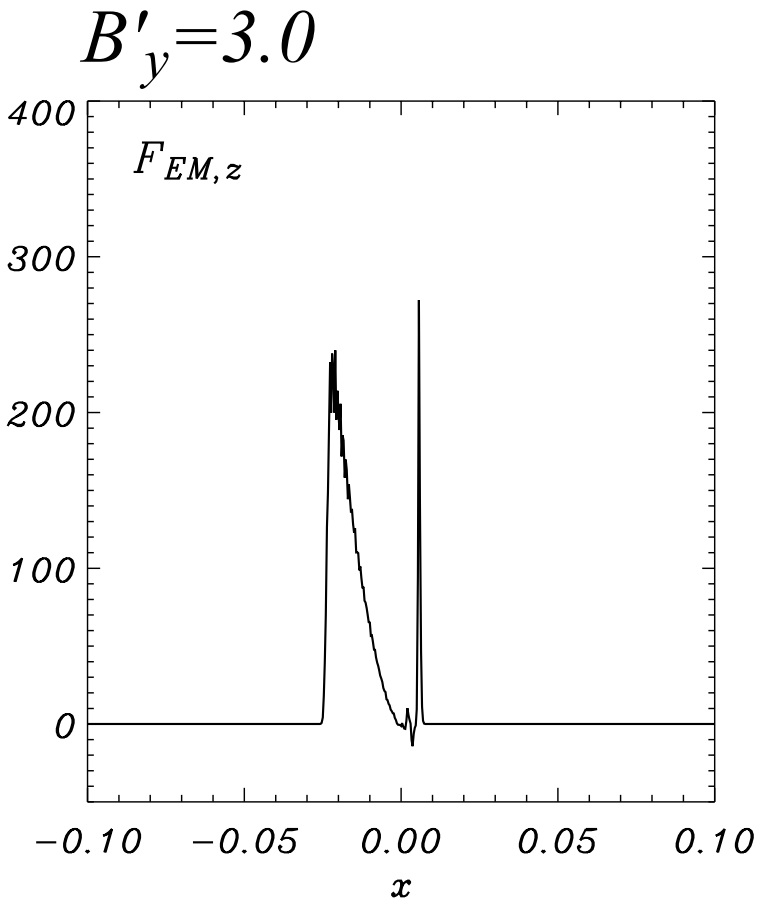

Fig. 4.— Profile of tangential component of Lorentz force ($F_{EM,z} = (\mathbf{J} \times \mathbf{B})_z$) of the MHDB ($B_y^{'} = 3.0$) case at time $t = 0.1$.

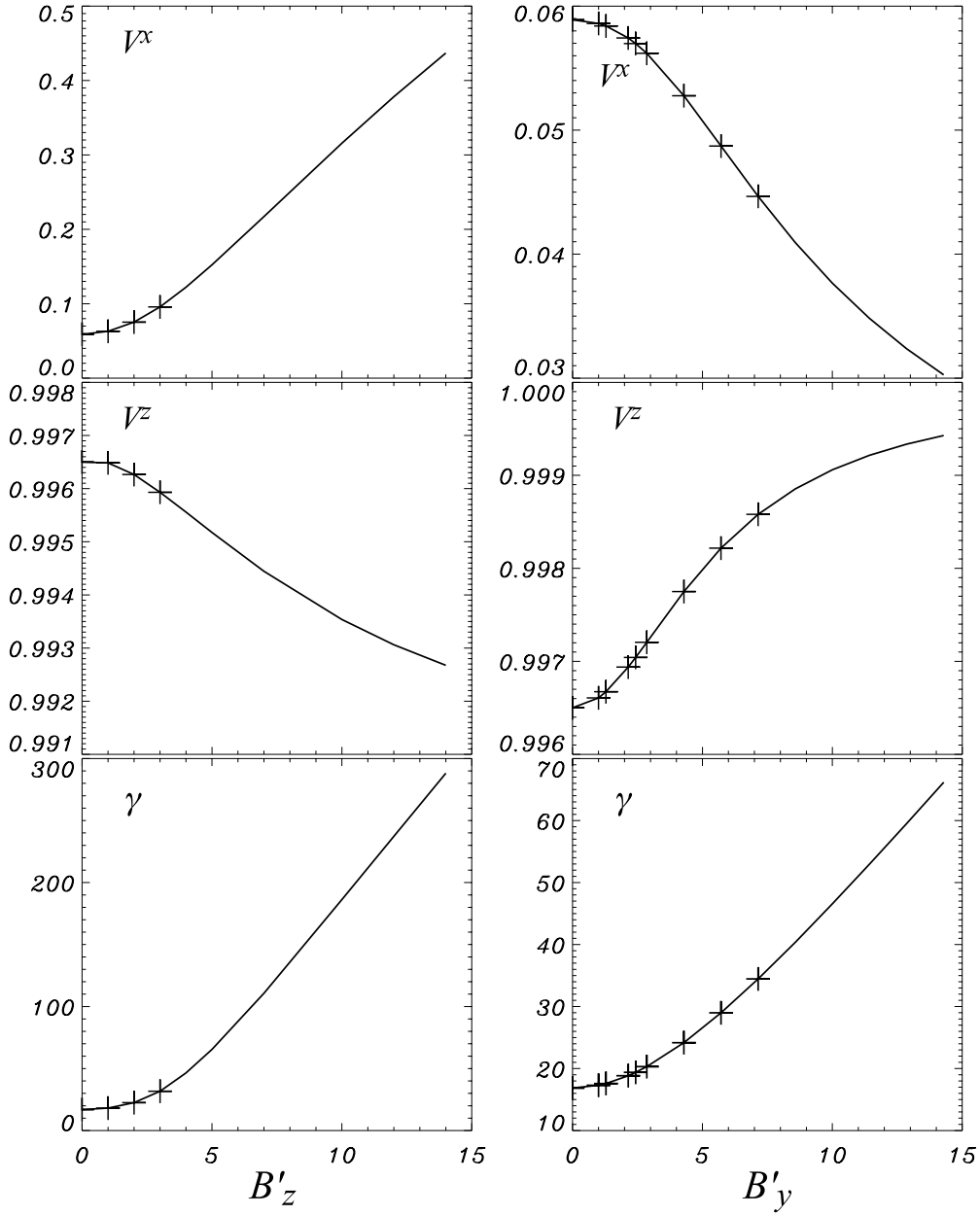

Fig. 5.— Dependence of maximum normal velocity (v^x) (*upper panel*), maximum tangential velocity (v^z) (*middle panels*) and maximum Lorentz factor $\gamma = [1-(v^x)^2-(v^z)^2]^{-1/2}$ (*lower panels*) on the strength of z-component of magnetic field $B_z^{'}$ (*left panels*) and y-component of magnetic field $B_y^{'}$ (*right panels*). The solid line indicates values obtained using the code of Giacomazzo & Rezzolla (2006) and the crosses indicate the values obtained from our simulations at the time $t = 0.1$.

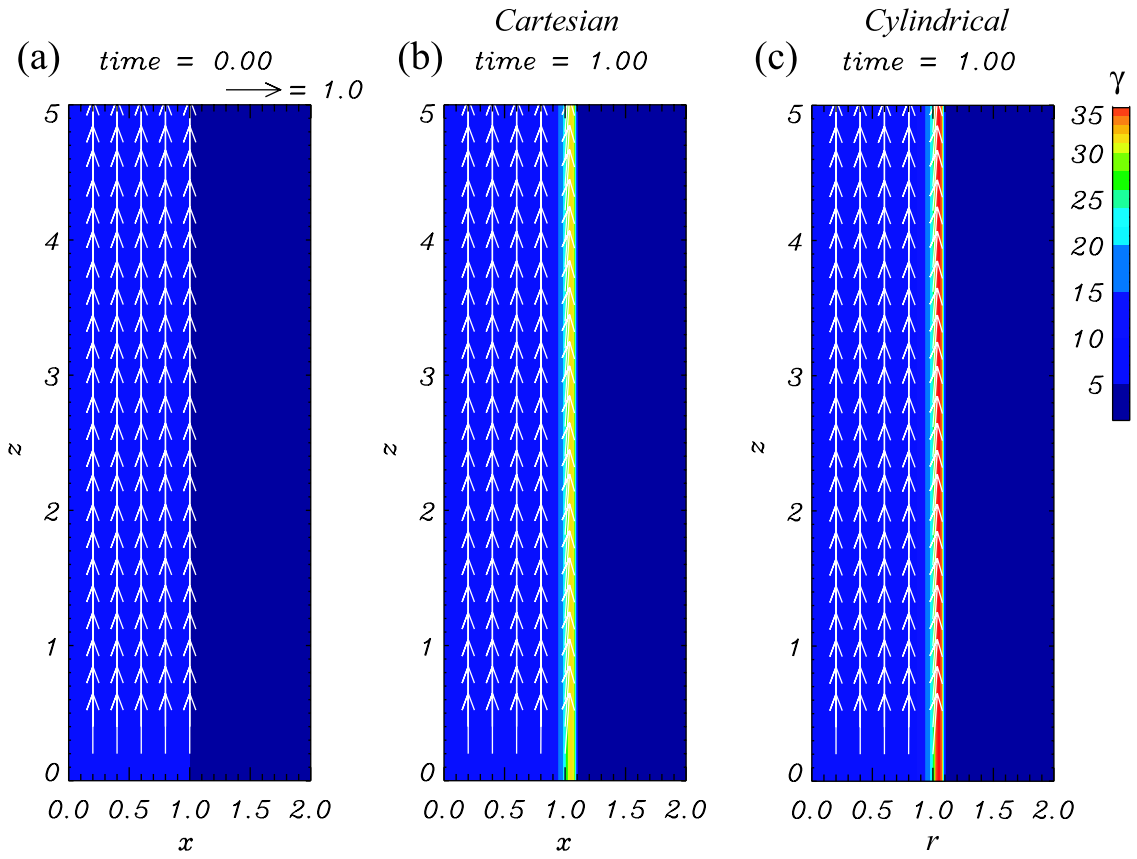

Fig. 6.— 2D images of Lorentz factor of (a) initial condition, (b) results of 2D MHDA in Cartesian coordinates case at time $t = 1.0$ and (c) results of 2D MHDA in cylindrical coordinates case at time $t = 1.0$. The color scales show the Lorentz factor. Arrows dipict the poloidal velocities normalized to light speed.

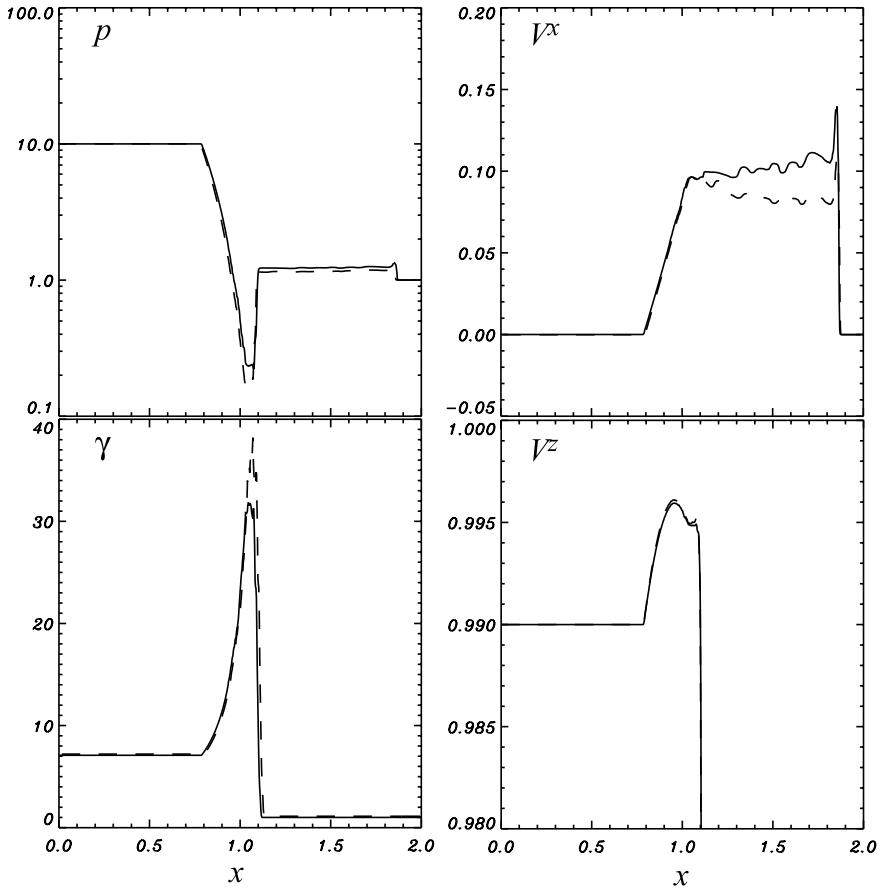

Fig. 7.— Profiles of (*left-upper panel*) density, (*left-lower panel*) Lorentz factor, (*right-upper panel*) normal velocity (v^x), and (*right-lower panel*) tangential velocity (v^z) of 2D MHDA ($B^z = 3.0$) in Cartesian coordinates (*solid lines*) and 2D MHDA in cylindrical coordinates (*dashed lines*) cases at time $t = 1.0$.